Metal-oxide supported Pt overlayers as Proton Exchange Membrane Fuel Cell cathodes

Vladimir Tripković[a], Frank Abild-Pedersen[a], Felix Studt[a], Isotta Cerri[b*], Tetsuo Nagami[c], Thomas Bligaard[a,d], Jan Rossmeisl[a,e]

[a] Computational Materials Design Aps, Lyngby, Denmark

[b] Toyota Motor Europe, Zaventem, Belgium

[c] Toyota Motor Corporation, Toyota-City, Japan

[d] Department of Chemical Engineering, Stanford University, Stanford, CA 94305 and Center for Interface Science and Catalysis, SLAC National Accelerator Laboratory, 2575 Sand Hill Rd, Menlo Park, CA 94025, USA

[e] Center for Atomic-scale Materials Design (CAMD), Department of Physics, Technical University of Denmark, DK-2800 Lyngby, Denmark

In the present work we have investigated the activity and stability of n = {1,2,3} platinum layers supported on a number of rutile metal-oxides MO_2 (M=Ti, Sn, Ta, Nb, Hf, Zr). A suitable oxide support can alleviate the problem of carbon corrosion and platinum dissolution in Pt/C catalysts. Moreover, it can also increase the activity of platinum if the interaction between the support and the metal is optimal. We find that both, activity and stability depend on the number of platinum layers and as expected, both converge to the bulk values when the number of layers is increased. Using a simple volcano picture for activity estimation, we find that supported platinum layers could be very active for oxygen reduction reaction and few of the candidates even surpass Pt. Furthermore, we have established a correlation between stability and activity, suggesting that activity can be increased at the expense of stability and vice versa. A tradeoff between the two properties will therefore yield an optimal catalyst. Finally, the performance of the systems was evaluated against Pt skins on Pt_3X (X = Ni, Co, Fe, Cu, Ti, Sc, Y) which are the best catalysts known to date for the reaction.

Published in ChemCatChem

Work supported in part by US Department of Energy contract DE-AC02-76SF00515.

SLAC National Accelerator Laboratory, Menlo Park, CA 94025

*corresponding author: ***Isotta.Cerri@toyota-europe.com***

Introduction

Despite of 160 years since the advent of the Fuel Cell (FC) technology; the fundamental issues, that impede its large scale manufacture, still remain unsolved. The main problem of using Pt as the cathode material still continues to be a puzzle for the scientific community. Many research activities in the past concentrated on reducing Pt content in the Proton Exchange Membrane Fuel Cells (PEMFC). The principal approach to achieve this is to alloy platinum with some non-noble transition metal such as V, Cr, Fe, Ni, Co, Cu [1,2,3,4,5] or similarly, deposit thin metal overlayers onto less noble metal substrates [6,7,8]. Readily, great activity enhancements for the oxygen reduction reaction (ORR) have been reported for such catalysts. Unfortunately, most of these systems do not form stable alloys, given that the less noble component tends to segregate to the surface and leach over time [9,10]. Extraordinary stable and active Pt alloy catalysts have been recently reported [7]; however their performance under FC cathode conditions still remains to be tested. The long term goal would certainly be to completely eliminate platinum from the PEMFC electrodes. Some attempts have lately been made to synthesize precious metal free catalyst for the ORR, but poor stability and low site specific current densities proved to be the limiting factors [11].

In addition, there are several other problems that necessitate pursuit for new catalyst materials. The dissolution potential of Pt (~1.2 V) is relatively high compared to the operation potential of low temperature FCs (0.6-0.7 V). However, the ramping of the potential to open circuit voltage (OCV) potential, 1.1-1.2 V, during stop-and-go drive can speed up Pt leaching, which in turn, severely degrades catalyst performance [12]. Another notable problem associated with harsh operating conditions in PEMFCs is the corrosion of the carbonaceous support, which thermodynamically starts already at 0.207 V [13]. This represents a huge problem, since loss of the support surface area causes Pt particles to sinter and thus reduces the ORR activity over long cycling hours required for automotive applications [14,15,16].

The question that naturally imposes is: whether a change of the support material could prevent Pt leaching and carbon corrosion. To answer this, one first needs to list specific requirements that a good support should fulfil: it needs to be corrosion resistant at high voltages and low pH. It needs to bind platinum strongly enough to shift the dissolution

potentials to higher values in order to prevent Pt corrosion during stop-and-go runs. In addition, it needs to maintain or improve the assets of carbonaceous supports, such as the electron conductivity, porosity and surface area size [17].

It is not easy to satisfy all of these conditions simultaneously; nevertheless changing support material can open up an ample spectrum of possibilities for screening for new catalyst materials and if the interaction of the metal catalyst with the support is favourable enough, perhaps provide a solution to the ultimate challenge of replacing platinum in PEMFCs. Most of the research so far has been focused on oxide supports, such as SnO_2, TiO_2, WO_3, SiO_2, NbO_2 [18,19,20,21,22]. All of these supports are stable under corrosive conditions required for PEMFC operation, apart from WO_3 which dissolves moderately [23],and in most cases the specific activities, that is, the activities normalized per surface area, were higher than for the state-of-the-art, Pt deposited on Vulcan-C, catalyst. On the other hand, the conductivity of such supports is extremely low. Most of these oxides are insulators (TiO_2, SiO_2) or in the best case wide band gap semiconductors (WO_3, SnO_2, NbO_2). This problem can be efficiently tackled by adding a small amount of dopants to the supports [24,25,26]. Doping enhances oxides' conductivity by few orders of magnitude and even in some cases the conductivities surpass the conductivity of the Vulcan-C support (4 S cm^{-1}) [17].

A much harder problem to deal with is how to increase the specific surface area of the metal-oxides, which is typically much smaller compared to surface areas of carbonaceous supports [17,27]. This is in fact the reason why these oxide supports have low mass activities, even though their specific activities are very high. Furthermore, the small surface area facilitates Pt particles' sintering and thereby contributes significantly to the loss of active surface area. New synthesis methods for oxide supports are needed to overcome this problem [17]. One of the possible solutions is nanostructuring of the support. Preliminary research efforts, have shown promising results, however, further tests need to be made, particularly under real operating conditions [28,29,30].

In this work we explore the activity and stability of the ORR catalysts made of n = {1,2,3} platinum layers supported on a variety of metal-oxides with the MO_2 stoichiometry (M = Ti, Sn, Ta, Nb, Hf, Zr). The paper is organized as follows. First, the methodology and model used to simulate Pt layers on the metal-oxide supports is introduced. Secondly, the performance of the supported Pt layers with respect to the stability against dissolution

and ORR activity is presented. Thirdly, the electronic effects coming from the support are disentangled from the electronic effects arising from the compression of the platinum lattice. Finally, the results are summarized and benchmarked against Pt and, moreover the performance of such supported Pt monolayers is compared to the performance of Pt skins on Pt_3X (X = Ni, Co, Fe, Cu, Ti, Sc, Y) alloys, which are nowadays recognized as the best catalysts for the ORR.

Method

All the electronic structure calculations are carried out using Density Functional Theory (DFT), with the RPBE generalized gradient functional for exchange and correlation (31). Ionic cores and their interaction with valence electron states are described by Vanderbilt ultra-soft pseudo potentials (32) and the valence wave functions are expanded in a plane wave basis set using a kinetic energy cut-off of 340 eV and a density cut-off of 640 eV. The electronic density of the valence states is obtained by a selfconsistent iterative diagonalization of the Kohn-Sham Hamiltonian with Pulay mixing of the densities. The occupation of the one-electron states is calculated using a temperature of k_bT = 0.1 eV; and later all energies have been extrapolated to T = 0 K.

We used the periodic slab representation, where each slab consisted of three oxide layers stacked along the (110) direction, which is the most close-packed direction of the rutile structure. Neighbouring metal-oxide slabs are separated by more than 25 Å of vacuum in order to make room for the inclusion of Pt layers. The dipole correction was used in all cases to decouple the electrostatic interactions between the periodically repeated slabs. The optimized Pt RPBE lattice constant of 4.02 Å is used to model the Pt overlayers. The Brillouin-zones are all sampled using the Monkhorst-Pack scheme (33), although with different *k*-point samplings. The calculations on the bulk metal-oxides are performed using a 4x4x6 k-point grid, whereas the bulk platinum and the bare Pt layers are sampled using a 6x6x4 and 4x4x1 *k*-point sampling grid, respectively. The combined systems Pt layer/metal-oxide are calculated using a *k*-point sampling of 4x2x1. Each time, symmetry was applied to further reduce the number of k-points.

All calculations were performed using the Dacapo software package (34) integrated with the ASE simulation environment (35).

Model

In our study the rutile metal-oxides MO_2 (M=Ti, Sn, Ta, Nb, Hf, Zr) have been considered as supports for Pt overlayers. The calculated and experimental lattice parameters are compared in Table 1. As observed there is a very good agreement between the two groups. We note that, experimental results for HfO_2 and ZrO_2 are lacking, because the rutile structure is not the most stable crystalline phase for these oxides. HfO_2 and ZrO_2 are isomorphous and they crystallize in the monoclinic phase. However, for simplicity reasons and to establish general trends we will use the rutile structure for all the metal-oxides in this study.

The systems were modelled by adding n = {1,2,3} Pt(111) layers on top of the most stable (110) metal-oxide surface termination.

	Calculated /Å		Experimental/Å	
	a	c	a	c
TiO_2	4.678	2.977	4.594[36]	2.959
SnO_2	4.865	3.245	4.737[37]	3.186
TaO_2	4.997	2.891	4.709[38]	3.065
NbO_2	4.981	2.928	4.846[39]	3.032
HfO_2	4.902	3.244	-	-
ZrO_2	4.931	3.274	-	-

Table 1. The optimized lattice parameters of the metal-oxides in the rutile structure along with the experimental counterparts. For TaO_2 the theoretical value has been shown instead, due to the lack of the experimental data.

To avoid unphysical straining of the Pt(111) overlayers, a proper size unitcell of the MO_2 support structure is selected. The unit cell size contains 12 Pt atoms in the case of M

= {Ti, Ta, Nb} and 14 for M = {Hf, Sn, Zr}, where the number of Pt atoms depends on the oxide surface area. The representative structures for both groups are illustrated in Figure 1.

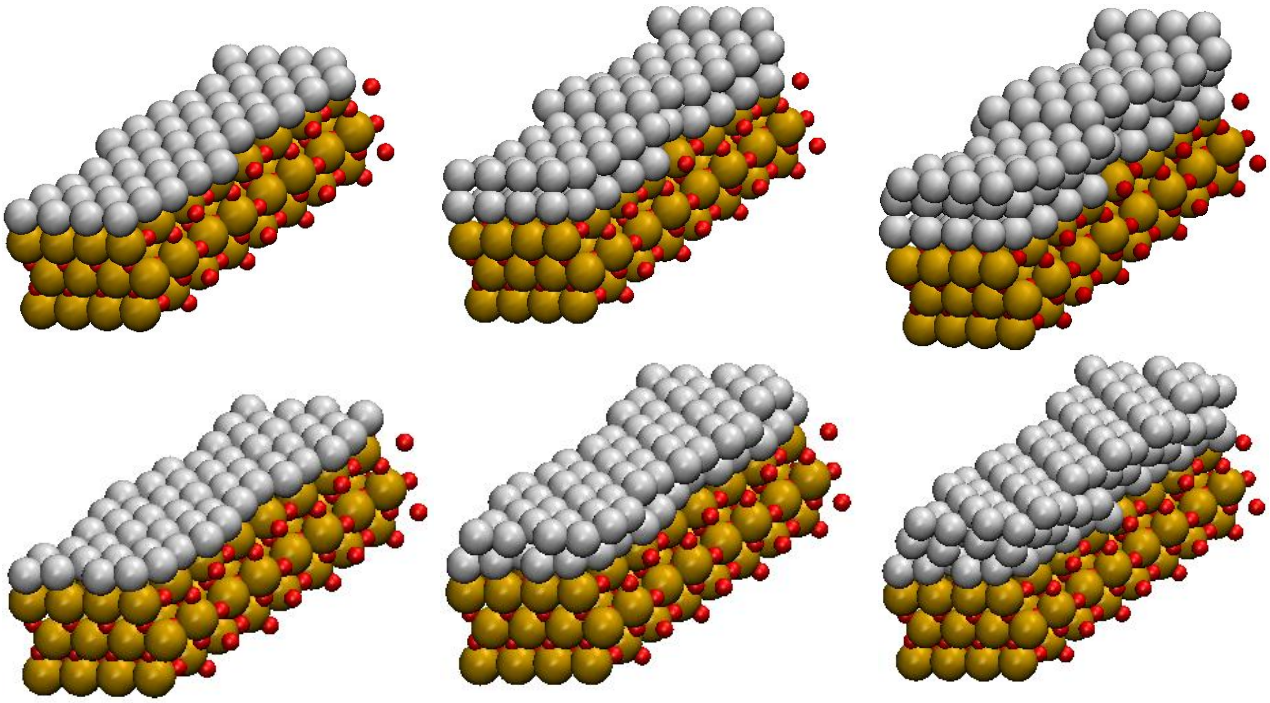

Figure 1. The illustrations of Pt monolayer (left), 2 layers (center) and 3 layers (right) on two representative metal-oxide supports having 12 (up) and 14 (bottom) Pt atoms in the unitcell, The platinum, oxide metal and oxygen atoms are represented by silver, brown and red balls, respectively.

To characterize the interface structure, we have calculated the interaction energy between the support and platinum layers, with and without the bridging oxygen atoms. In the former case, the adhesion between Pt(111) and the metal oxide is negligible which results in a complete separation of the two phases. Hence, we conclude that, in order to ensure binding between the two phases, the oxide surface must first be reduced.

To ensure convergence of adhesion energies, we have tested how many oxide layers are required before the change in Pt – metal oxide binding becomes negligible. Sufficient convergence is reached at 3 oxide layers (c. f. supplementary material).

Results and discussion

This section is organized in three parts. First, the results regarding the stability of the supported Pt overlayers are presented. Secondly, we present results of their specific theoretical ORR activities. Finally, the activity and stability are benchmarked versus platinum to pinpoint the best catalyst candidates, and in addition, compared against the best Pt-alloy catalysts for the reaction.

Stability

The corrosive PEMFC cathode working environment (high potential & low pH), imposes very stringent requirements on the stability. In the following, the stability of the metal oxides and platinum overlayers will be addressed. As mentioned in the introduction, TiO_2, SnO_2 are quite stable under these harsh operating conditions, as well are TaO_2 and NbO_2, that are produced from Ta_2O_5 and Nb_2O_5 at elevated temperatures under reducing conditions [40]. HfO_2 and ZrO_2 rutile structures can also be considered stable, since they are used as models for their stable monoclinic counterparts.

As stability descriptor we will use the dissolution potential of the supported Pt overlayers given with respect to bulk Pt as stated in Eq. 2.

$$E_{diss} = E_{diss}^{Pt_{bulk}} - \left[\left(E_{nPt(111)+MO_2} - E_{(n-1)Pt(111)+MO_2} - NE_{Pt_{bulk}} \right) / N \right] \qquad (2)$$

where n = {1,2,3} is the number of Pt layers and N = {12, 14} is the number of Pt atoms in each layer. According to the formula, the reduced metal-oxide surface is used as a reference in the case of the supported Pt monolayers. The calculated dissolution potentials are provided in Table 2 and graphically illustrated in Figure 2. These results are compared to 1.2 V, which is the dissolution potential of bulk Pt under standard conditions. It is important to stress that the dissolution potential of Pt nano particles will be lower than the bulk value due to the presence of highly undercoordinated defect sites. Lower values than 1.2 V favour formation

of the bulk phase i.e. sintering. Therefore the systems with values higher or at least close to 1.2 V are the systems we are particularly interested in.

Structure	Dissolution potential, V		
	1st Pt layer	2nd Pt layer	3rd Pt layer
TiO_2	1.09	0.83	1.05
SnO_2	0.83	0.77	1.02
TaO_2	2.01	0.85	1.16
NbO_2	1.58	0.84	1.16
HfO_2	1.75	0.64	1.05
ZrO_2	1.67	0.01	0.98

Table 2. *The calculated dissolution potentials for n = {1,2,3} Pt overlayers on the metal-oxide supports.*

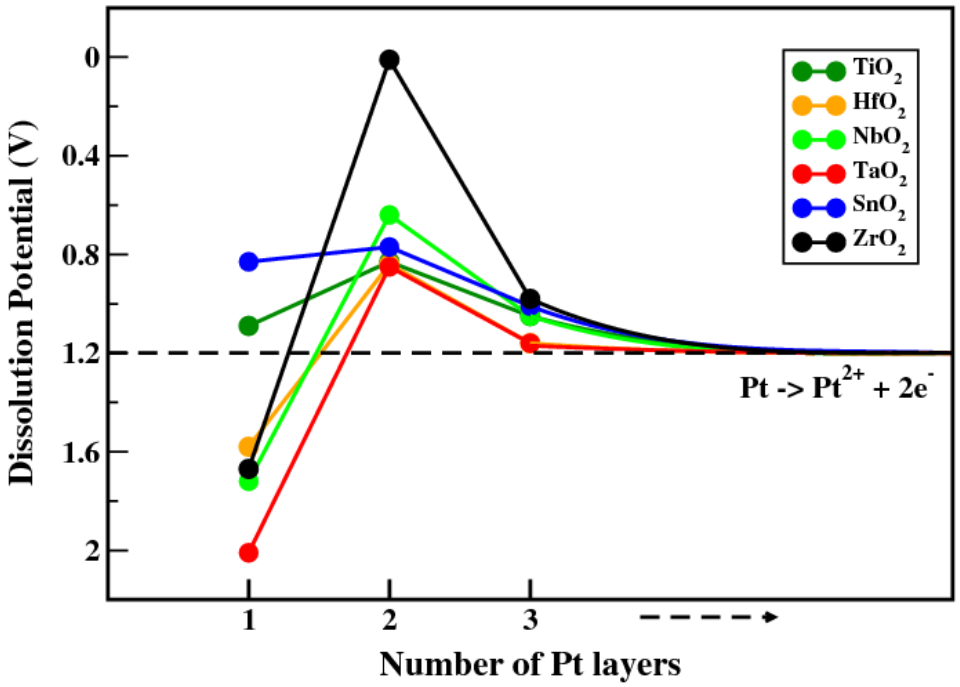

Figure 2. The dissolution potentials as a function of the number of Pt layers on the metal-oxides supports. The dashed line represents the dissolution potential of bulk Pt under standard conditions.

As seen, the overall trend in dissolution potentials behaves in the same way for all the metal-oxides. As more Pt layers are added, the dissolution potential approaches the dissolution potential of bulk Pt, 1.2 V. In the case of M = {Ta, Nb, Hf, Zr} the reduced metal oxides have high surface energies and hence they bind the first Pt layer very strongly, increasing the dissolution potential beyond 1.2 V. These systems will be very stable against sintering. When the second Pt layer is added, the dissolution potential falls significantly and in all the cases it becomes much less than 1.2 V, implying that the Pt atoms will have a propensity to sinter over time. After addition of the third layer, the dissolution potentials increase again and approach the bulk dissolution value. This behavior can be easily interpreted through the effective medium theory reckoning: the first platinum layer is very strongly bonded to the support, thus it has less available electron density to bind to the second layer. This effect will gradually die off as the number of layers is increased; that is, the effect of the support will become shielded and consequently the dissolution potential will converge to the bulk value. Evidently, the convergence is almost reached after addition of the third platinum layer. In most cases the most stable systems are the ones with adsorbed Pt monolayer.

Activity

Interplay between theory and experiments plays a significant role in modern catalyst design. One of the most important contributions from DFT calculations is the establishment of the 1st order scaling relations between binding energies of reaction intermediates [41,42,43]. These relations give rise to volcano curves, where the intermediates' binding energies can be used as unique descriptors for activity [44,45,46,47,48]. Such relationships are indeed very useful, since only few parameters need to be determined to get the overall activity prediction. The use of DFT calculations has thus paved a way to numerous screening studies, which have pinpointed better catalytic materials for a number of reactions [10,49,50]. More specifically in the case of the ORR, the oxygen binding energy was found to be a single descriptor determining the overall activity [45]. According to this methodology, the ORR activity can be accurately estimated by oxygen binding energy alone.

After investigating all possible adsorption sites for oxygen binding (top, bridge, fcc and hcp), it was found, that oxygen prefers the fcc adsorption site in almost all cases. The oxygen binding energies are calculated with respect to to H_2O(l) and H_2(g), as in ref. [45], and listed in Table 3. The results for the oxygen adsorption on 2 & 3 platinum layers supported on SnO_2 are not included because these systems were found to be unstable.

Structure	Oxygen adsorption energy, eV		
	1st Pt layer	2nd Pt layer	3rd Pt layer
TiO_2	1.84	1.66	1.52
SnO_2	2.20	-	-
TaO_2	2.38	1.80	1.74
NbO_2	2.11	1.75	1.71
HfO_2	2.09	1.82	1.44*
ZrO_2	2.33	2.01	1.88

Table 3. The oxygen adsorption energies relative to H_2O(l) and H_2(g) on n = {1,2,3} platinum layers supported on the metal-oxides. The asterisk denotes the bridge adsorption site (in all other cases the fcc site is the most stable adsorption site). For comparison, the value of the oxygen adsorption energy on a bare Pt(111) surface is 1.53 eV.

In an attempt to disentangle the electronic effects coming from the substrate from the electronic effect coming from the compression of the Pt lattice, we have calculated the oxygen binding energy on the compressed Pt(111) layer in the metal-oxide unit cell, without the substrate. The differences between the oxygen binding energies on Pt with and without the substrate will quantify the impact of both effects. The larger the difference, the more pronounced the influence of the support is. As seen in Figure 3, the substrate's electronic effect plays a dominant role only in the case of a Pt monolayer supported on NbO_2 and TaO_2. For the other metal oxides considered, it is rather small and with addition of more layers it becomes even less pronounced.

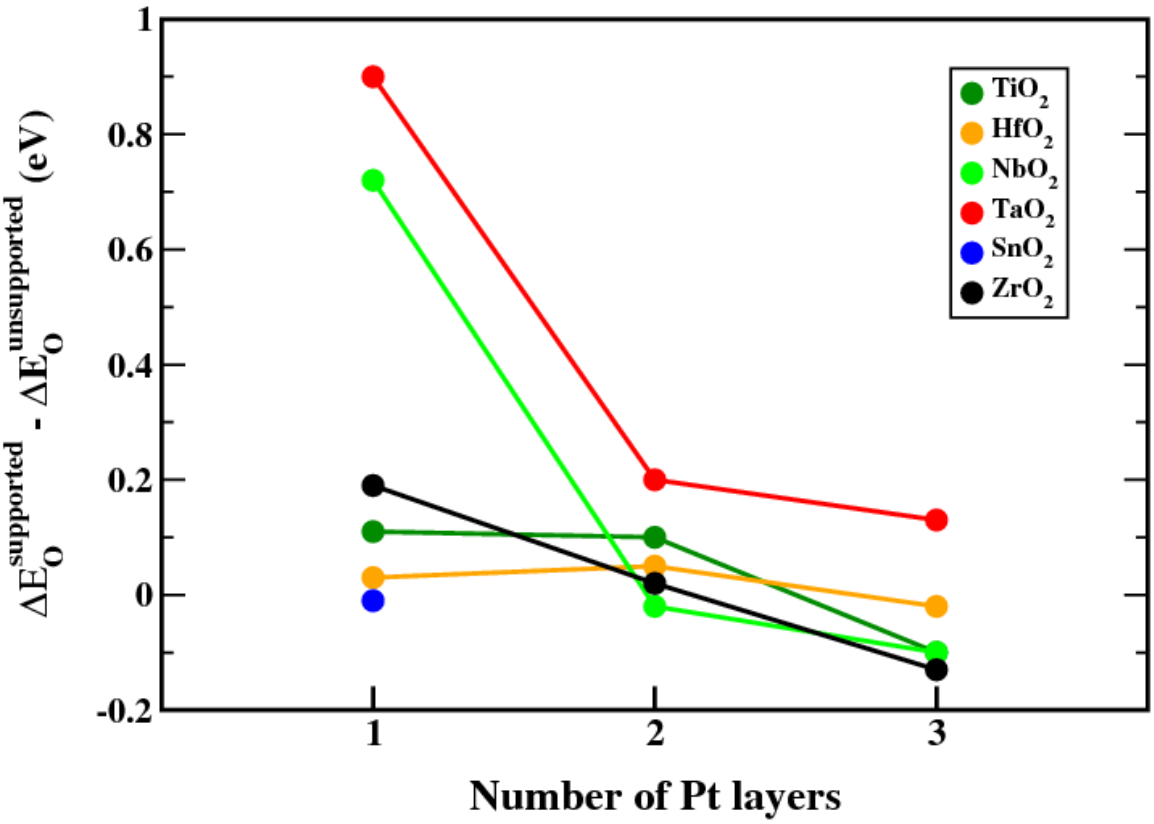

Figure 3. Difference between the oxygen binding energies on the supported and not supported Pt layers as a function of the number of Pt layers. The difference indicates which effect prevails; the electronic effect coming from the support or the electronic effect coming from the compressed Pt lattice.

The volcano plots based on the calculated oxygen binding energies normalized with respect to Pt(111) are shown in Figure 4. Since the apex of the volcano lies 0.2 eV to the right from the oxygen binding energy on platinum, we are mostly interested in materials that bind oxygen somewhat weaker than Pt(111).

The same argument that was used to explain the trend in dissolution potentials (stability) can just as well be applied to describe trends in the oxygen binding energies (activity). Namely, weaker bound n = {2,3} Pt overlayers bind oxygen more strongly than tightly bound single Pt overlayer. As a result, the activity of the supported Pt monolayers shifts very much to the right, far from the volcano top. This is also manifested in a strong lattice compression which varies between 1% (HfO_2) and 8%

(SnO_2) as seen in Table 5. After addition of a second and third Pt layer, the oxygen binding energy increases on all the systems shifting the values within the optimum range.

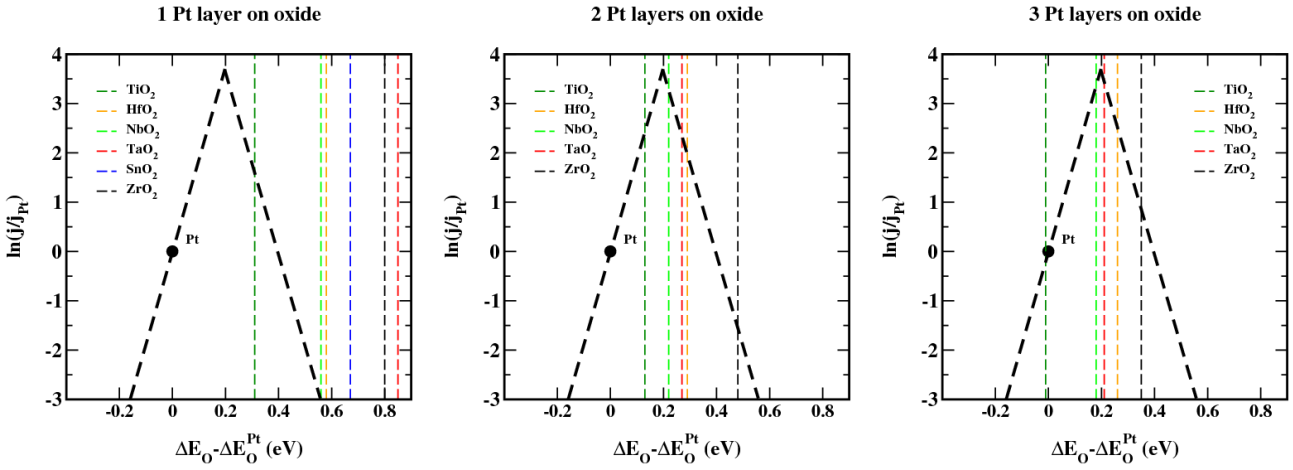

Figure 4. The ORR activity as a function of the oxygen binding energy on the supported 1 (left) 2 (center) and 3 (right) Pt layers, relative to Pt(111). The binding energies are indicated by the dashed vertical lines that give an estimate of the activity at the point of intercept with the volcanoes.

Activity vs Stability

The best way to evaluate catalysts is to plot their general properties, such as stability, activity and cost, against each other. Since all of the oxide supports are rather cheap compared to the platinum metal, the cost can be removed from the equation.

The activity vs stability plot is shown in Figure 5. For the moment we will focus on the performance of the metal-oxide systems denoted by circles with numbers. The first platinum layer on the metal-oxides is more stable than bulk Pt, but it exhibits a very poor activity. On the other hand, the second layer is quite active, but unstable and over time the platinum atoms would agglomerate into particles. The systems with 3 Pt layers seem to be the most promising ones, since they are fairly stable and extremely active. However, being slightly less stable than bulk Pt, they would presumably agglomerate to nanoparticles in time.

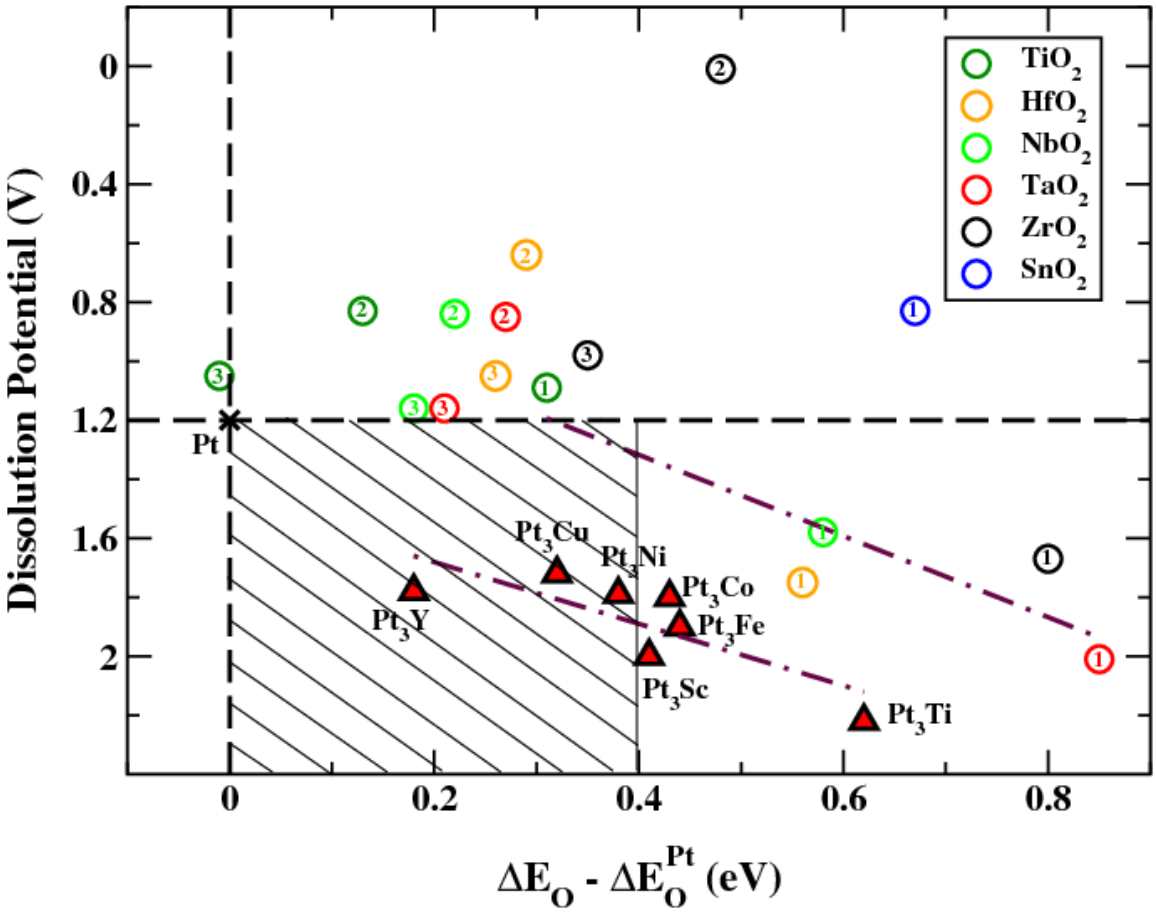

Figure 5. The stability (dissolution potential) is plotted versus the activity (oxygen binding energy). The oxygen binding energies are shown with respect to Pt(111). The two dashed lines are indicated for comparison and they represent the activity corresponding to Pt(111) and the dissolution potential of bulk Pt. The hatched box designates the area containing the best catalyst materials. The empty circles with numbers and filled triangles represent the metal-oxide and Pt/Pt_3X data points, respectively. The two brown dashed-doted lines are the fits for the supported Pt monolayers on the metal-oxides (without SnO_2) and alloys.

The ideal catalyst should fall in the hatched area designated in Figure 5. The hatched area ranges from the oxygen binding energy on a bare Pt(111) surface to the symmetrical point on the right leg of the volcano. At the same time the preferable dissolution potential should be higher than for the bulk Pt (ca. 1.2 V). As seen, none of the investigated systems fall into this area; however, there are two candidates (3 Pt layers

supported on NbO_2 & TaO_2) that reside just outside of the rim of the hatched box. In fact, a thin Pt layer deposited on NbO_2 has been found experimentally to be quite active for the ORR [12,27].

Another important observation is that an increase in the activity will produce a decrease in the stability for supported Pt(111) monolayers. The linear relationship between the stability and activity suggests that for a single Pt(111) layer, the dissolution potential might be a reasonable descriptor for the activity as well. When more layers are added, the dissolution potential becomes fairly constant due to the above mentioned shielding effect and for the same reason the activity approaches that of Pt(111). Here, it is important to stress that the linear relationship drawn for the metal-oxide systems is perhaps not the best way to correlate the points. Pt monolayers on Hf, Zr and Sn oxides, that comprise 14 Pt atoms, deviate from the linear behaviour. However, it is instructive to keep the linear trend for all the metal-oxides in order to make a comparison against the alloy systems.

At this point we turn back our attention to the Pt skins on alloys denoted by black filled triangles in Figure 5. It is clearly seen from the fits that the trend is the same for the two different systems, suggesting a more general rule that one cannot promote activity without simultaneously sacrificing stability. The second observation is that Pt skins are ca. 0,5 eV more stable than Pt overlayers on the metal-oxides and that most of them fall in the hatched area. This explains the exceptional performance of these materials for the ORR. Clearly, it is much easier to accommodate a single Pt layer on Pt alloys, which have the same stacking order as Pt, than on the metal-oxides with completely different unitcells. The mismatch between the (110) rutile unitcell and (111) Pt lattice produces large strain effects that result in a substantial system destabilization. One could, in principle, think of some other oxide substrates than rutile that would better fit Pt overlayers and consequently increase the stability. The stability of the Pt skins is obviously the maximum that could be attained, since it would be hard to imagine any other substrate material that would produce less strain in Pt overlayers compared to Pt_3X alloys. Now, as activity is concerned, the metal-oxide supported Pt monolayers are somewhat less active than the Pt alloys, given that they bind oxygen slightly more weakly. This is mainly due to a larger compression of the Pt lattice induced on the metal-

oxides. The relative strains of the metal-oxides and Pt_3X alloys supported Pt monolayers, calculated from Eq. (1), are summarized in Table 4.

$$\text{strain}\,(\%) = \frac{a_{Pt(MO_2/Pt_3X)}}{a_{Pt}} \qquad (1)$$

where $a_{Pt(MO_2/Pt_3X)}$ and a_{Pt} are the lattice constants of the supported Pt monolayers and bulk Pt, respectively.

Metal-oxides	**TiO_2**	**SnO_2**	**TaO_2**	**NbO_2**	**HfO_2**	**ZrO_2**	
strain (%)	0.94	0.92	0.96	0.98	0.99	0.93	
Alloys	**Pt_3Ni**	**Pt_3Co**	**Pt_3Cu**	**Pt_3Fe**	**Pt_3Ti**	**Pt_3Sc**	**Pt_3Y**
strain (%)	0.98	0.98	0.98	0.99	0.99	1.01	1.04

Table 4. Relative strains of Pt lattices, according to Eq. (1), for Pt monolayers supported on the metal-oxides and Pt_3X alloys

The last issue that will be tackled here is the possibility of promoting the stability and activity of the bare oxide supports by adding a small amount of dopants. In that regard, we have calculated the lattice parameters and dissolution potentials of doped metal oxides. We have considered TiO_2 doped with {Nb, Ta, and W}, SnO_2 with {In, P, and Sb} and NbO_2 with {Hf, W, and Zr}. The concentration of the doped material was kept low at 1/16, corresponding to 1 dopant per unit cell. The dopant was placed in the second layer instead of the metal atom in the metal-oxide support. The values of the lattice parameters and dissolution potentials can be found in the supplementary material. The general observation is that the low concentration doping does not affect lattice parameters and dissolution potentials. This finding is yet another indicator that the electronic effects coming from the lattice compression, rather than intrinsic electronic effects, play a crucial role in determining the stability and activity of platinum overlayers, (cf. Figure 3). As mentioned in the introduction, the doping might be inevitable from another point of view, namely, it increases the number of charge carriers and thereby also the conductivity of oxide supports sometimes even by several orders of magnitude.

Conclusion

In the work presented, we have analyzed the influence of the metal-oxide substrates on the activity and stability of n = {1,2,3} Pt(111) overlayers supported on the different metal-oxides. We conclude that the most promising systems are the 3Pt layers supported on NbO_2 and TaO_2. They are extremely active, a little bit less stable than bulk platinum, albeit presumably more stable than Pt nano particles. Even so they present very good candidates to be tested in experiments.

Another important observation is that the activity and stability scale inversely for the supported Pt monolayers on both metal-oxides and Pt_3X alloys; implying a general rule that a more active catalyst is at the same time less stable.

Furthermore, it has also been demonstrated that the compression of Pt lattice due to the support is the main effect responsible for the improved activity of the supported Pt overlayers. On the other hand, the same effect produces large strains which disrupt and destabilize Pt overlayers on the metal-oxides, rendering them some 0,5 eV less stable than the same overlayers on Pt_3X type alloys. A possible solution might be in finding the appropriate substrate surface that could attenuate the strain and bring the stability closer to Pt_3X.

We would like to emphasize that even though the study was focused on platinum overlayers, it could be readily extended to other supported metals as well. Particularly interesting would be the early transition metals which are known to bind oxygen too strongly and to dissolve under PEMFC conditions. The stronger binding to the support could in principle enhance the activity by weakening the oxygen binding energy and shifting it towards the optimum range (~1.50-1.90 eV). At the same time, the dissolution potentials would increase significantly and potentially become equal or higher than Pt bulk. However, one cannot *apriori* predict how the metal lattice and hence the ORR activity and stability would be affected and besides these metals might self turn to oxides under oxidizing conditions.

Finally, the low concentration doping will not have large impact on the catalytic behaviour of these systems, taking into account that the electronic influence of the

substrate is rather small compared to the lattice compression caused by the lattices' mismatch.

The adhesion of metal overlayers is still an uncharted area and hence it offers many possibilities for catalyst design, not just for the oxygen reduction, but generally for all other catalytic reactions. Exploring new areas is essential for achieve breakthroughs that could potentially lead to a new generation of cheaper, more active, and more durable catalysts.

Acknowledgments

We greatly acknowledge support from Toyota Motor Europe.

Supporting information

SI 1:

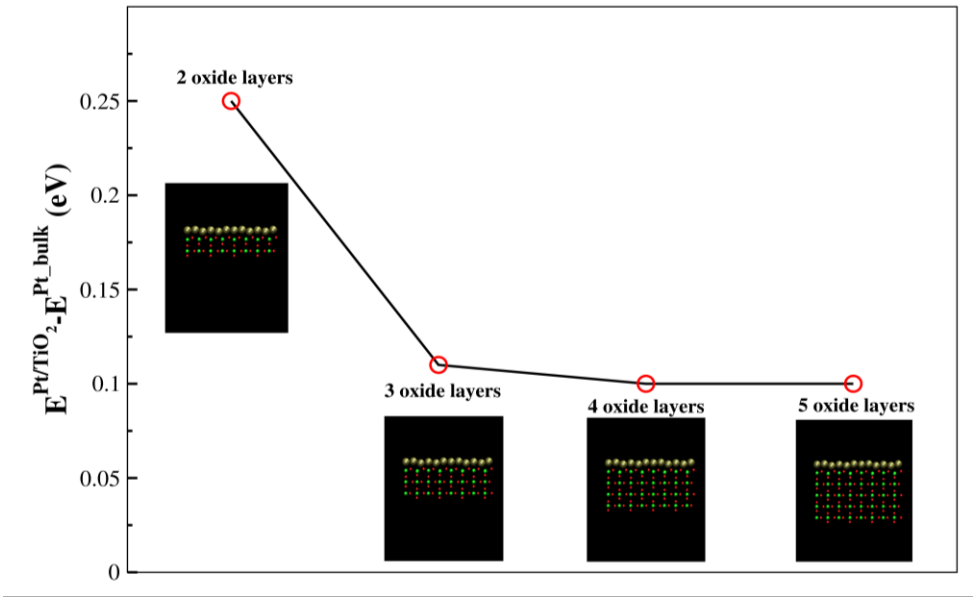

Figure 6. The stability of Pt monolayer on TiO_2 as a function of the number of metal-oxide layers.

SI 2:

We have calculated the phase diagrams, lattice parameters and dissolution potentials for doped metal-oxides. We have initially considered TiO_2 doped with {Nb, Ta, and W}, SnO_2 with {In, P, and Sb} and NbO_2 with {Hf, W, and Zr}. The concentration of dopants was 1/16 (1 dopant per unit cell). The dopant atom was placed instead of the metal atom in the second layer of the metal-oxide support.

Although we have considered 9 different doped systems, here we show results for lattice constants and dissolution potentials only for 5 that were found to be stable at U = 1.2 V & pH = 0.

Structure	a (Å)	b (Å)	c (Å)
Nb/TiO_2	4.700	4.700	2.985
W/TiO_2	4.695	4.695	2.984
Sb/SnO_2	4.871	4.871	3.255
W/NbO_2	4.980	4.980	3.050
Zr/NbO_2	4.988	4.988	3.050

Table 5 *Calculated lattice constants for stable doped TiO_2, SnO_2 and NbO_2.*

Structure	1st layer		2nd layer		3rd layer	
	(111)	(100)	(111)	(100)	(111)	(100)
Nb/TiO_2	1.11	0.54	0.83	0.91	1.04	1.08
W/TiO_2	1.10	0.54	0.83	0.95	1.04	1.05
Sb/SnO_2	0.83	0.32	0.78	0.81	1.00	1.04
W/NbO_2	1.56	1.49	0.79	0.73	1.15	1.05
Zr/NbO_2	1.55	1.49	0.78	0.71	1.14	1.08

Table 6 *Calculated dissolution potentials for stable doped TiO_2, SnO_2 and NbO_2.*

References

1 S. Mukerjee, S. Srinivasan, *J. Electroanal. Chem.* **357** (1993) 201.

2 V. R. Stamenkovic, B. Fowler, B. S. Mun, G. Wang, P. N. Ross, C. A. Lucas, N. M. Markovic, *Science* **315** (2007) 493.

3 V. R. Stamenkovic, B. S. Mun, M. Arenz, K. J. J. Mayrhofer, C. A. Lucas, G. Wang, P. N. Ross, N. M. Markovic, *Nature* **6** (2007) 241.

4 A. U. Nilekar, Y. Xu, J. Zhang, M. B. Vukmirovic, K. Sasaki, R. R. Adzic, M. Mavrikakis, *Top. Catal.* **26** (2007) 276.

5 S. Koh, P. Strasser, *J. Am. Chem. Soc.* **129** (2007) 12624.

6 J. Zhang, M. B. Vukmirovic, K. Sasaki, A. U. Nilekar, M. Mavrikakis, R. R. Adzic, *J. Am. Chem. Soc.* **127** (2005) 12480–12481.

7 J. Zhang, Y. Mo, M. B. Vukmirovic, R. Klie, K. Sasaki, R. R. Adzic, *J. Phys. Chem. B* **108** (2004) 10955–10964.

8 J. Zhang, F. H. B. Lima, M. H. Shao, K. Sasaki, J. X. Wang, J. Hanson, R. R. Adzic, *J. Phys. Chem. B* **109** (2005) 22701.

9 H. A. Gasteiger, S. S. Kocha, B. Sompalli, F. T. Wagner, *App. Caalt. B - Env* **56** (2005) 9.

10 J. Greeley, I. E. L. Stephens, A. S. Bondarenko, T. P. Johansson, H. A. Hansen, T. F. Jaramillo, J. Rossmeisl, I. Chorkendorff, J. K. Nørskov, *Nature Chem.* **1** (2009) 552.

11 M. Lefèvre, E. Proietti, F. Jaouen, J.-P. Dodelet, *Science* **71** (2009) 324.

12 K. Sasaki, L. Zhang, R. R. Adzic, *Phys. Chem. Chem. Phys.* **10** (2008) 159.

13 M. Pourbaix, Atlas of Electrochemical Equilibria in Aqueous Solution, National Association of Corrosion Engineers, Houston, TX, 1979.

14 G. A. Gruver, *J. Electrochem. Soc.* **125** (1978) 1719.

15 P. Stonehart, *Carbon* **22** (1984) 423.

16 J. Wang, G. Yin, Y. Shao, S. Zhang, Z.Wang, Y. Gao, *J. Power Sources* **171** (2007) 331.

17 E. Antolini, E. R. Gonzalez, *Solid State Ionics* **180** (2009) 746

18 T. Ioroi, Z. Siroma, N. Fujiwara, S. Yamazaki, K. Yasuda, *Electrochem. Comm.* **7** (2005) 183

19 N. R. Elezovic, B. M. Babic, V. R. Radmilovic, Lj. M. Vracar, N. V. Krstajic, *Electrochem. Acta* **54** (2009) 2404.

20 T. Ioroi, H. Senoh, S. Yamazaki, Z. Siroma, N. Fujiwara, K. Yasuda, *J. Electrochem. Soc.* **155** (2008) B321.

21 B. Seger, A. Kongkanand, K. Vinodgopal, P. V. Kamat, *J. Electroanal. Chem.* **621** (2008) 198.

22 H. Chhina, S. Campbell, O. Kesler, *J. Electrochem. Soc.* **154** (2007) B533.

23 B. Reichman, A. J. Bard, *J. Electrochem. Soc.* **126** (1979) 583.

24 M. S. Saha, R. Li, M. Cai, X. Sun, *Electrochem. Solid State Lett.* **10** (2007) B130.

25 K.-W. Park, K.-S. Seol, *Electrochem. Comm* **9** (2007) 2256.

26 O. E. Haas, S. T. Briskeby, O. E. Kongstein, M. Tsypkin, R. Tunold, B. T. Børresen, J. New Mater. *Electrochem. Syst.* **11** (2008) 9.

27 L. Zhang, L. Wang, C. M. B. Holt, T. Navessin, K. Malek, M. H. Eikerling, D. Mitlin, *J. Phys. Chem. C* **114** (2010) 16463.

28 S. H. Kang, T.-Y. Jeon, H.-S. Kim, Y.-E. Sung, W. H. Smyrl, *J. Electrochem. Soc.***155** (208) B1058.

29 S. H. Kang, Y.-E. Sung, W. H. Smyrl, *J. Electrochem. Soc.* **155** (2008) B1128.

30 M. S. Saha, R. Li, M. Cai, X. Sun, Electrochem. *Solid State Lett.* **10** (2007) B130.

31 B. Hammer, L. B. Hansen, J. K. Nørskov, *Phys. Rev. B* **59** (1999) 7413.

32 D. Vanderbilt, *Phys.Rev. B* **41** (1990) 7892.

33 H. J. Monkhorst, J. D. Pack, *Phys. Rev. B* **13** (1976) 5188.

34 *Dacapo pseudopotential code, URL: https.//wiki.fysik.dtu.dk/dacapo, Center for Atomic Scale Materiale Design (CAMD), Technical University of Denmark, Lyngby.*

35 *Atomic Simulation Environment (ASE), URL: https/wiki.fysik.dtu.dk/ase, Ceter for Atomic Scale Materiale Design (CAMD), Technical University of Denmark, Lyngby.*

36 C. J. Howard; T. M. Sabine; F. Dickson, *Acta. Cryst.* **47** (1991) 462.

37 A. A. Bolzan, C. Fong, B. J. Kennedy, C. J. Howard, *Acta. Cryst.* **373** (1997) B53.

38 M. Kitamura, K. Inoue, H. Chen, Materials Chemistry and Physics 56 (1998) 1.

39 A. A. Bolzan; C. Fong, B. J. Kennedy, C. J. Howard, *J. Solid State Chem.* **113** (1994) 9.

40 C. K. Gupta, A. K. Sun, *Extractive Metallurgy of Niobium*, CRC press 1994.

41 F. Abild-Pedersen, J. Greeley, F. Studt, J. Rossmeisl, T. R. Munter, P.G. Moses, E. Skúlason, T. Bligaard, J. K. Nørskov, *Phys. Rev. Lett.* **99** (2007) 016105.

42 G. Jones, F. Studt, F. Abild-Pedersen, J. K. Nørskov, T. Bligaard, *Chem. Eng. Sci.* (2011), doi:10.1016/j.ces.2011.02.050.

43 J. Rossmeisl, A. Logadottir, J. K. Nørskov, *J. Chem. Phys.* **319** (2005) 178.

44 J. K. Nørskov, T. Bligaard, A. Logadottir, J. R. Kitchin, J. G. Chen, S. Pandelov, U. Stimming, *J. Electrochem. Soc.* **152** (2005) J23.

45 J. K. Nørskov, J. Rossmeisl, A. Logadottir, L. Lindqvist, J. R. Kitchin, T. Bligaard, H. Jónsson, *J. Phys. Chem. B* **108** (2004) 17886.

46 J. Rossmeisl, Z.–W. Qu, H. Zhu, G.-J. Kroes, J. K. Nørskov, *J. Electroanal. Chem.* **607** (2007) 83.

47 C. J. H. Jacobsen, S. Dahl, B. S. Clausen, S. Bahn , A. Logadottir , J. K. Nørskov, *J. Am. Chem. Soc.* **123** (2001) 8404.

48 J. Kleis, G. Jones, F. Abild-Pedersen, V. Tripkovic, T. Bligaard, J. Rossmeisl, *J. Electrochem. Soc.* **156** (2009) B1447.

49 J. Greeley, T. F. Jaramillo, J. Bonde, I. Chorkendorff, J. K. Nørskov, *Nature materials* **5** (2006) 909.

50 F. Studt, F. Abild-Pedersen, T. Bligaard, R. Z. Sørensen, C. H. Christensen, J. K. Nørskov, *Science* **320** (2008) 1320.